Chinese Journal of Natural Medicines

Targeting of MARK2, but not other MARKs, suppresses TNBC progression by inhibition of the mutant p53–driven signaling pathway

Min Zhang, Xilong Zhu, Mengqian Cui, Yinan Guan, Yong Zhang, Stephen J Weiss, Jun Chen, Yongzhong Yao, Rong Fu, Zhaoqiu Wu

Citation: Min Zhang, Xilong Zhu, Mengqian Cui, Yinan Guan, Yong Zhang, Stephen J Weiss, Jun Chen, Yongzhong Yao, Rong Fu, Zhaoqiu Wu, Targeting of MARK2, but not other MARKs, suppresses TNBC progression by inhibition of the mutant p53–driven signaling pathway, Chinese Journal of Natural Medicines, 2026, 24(4), 414–426. doi: 10.1016/S1875–5364(26)61172–7.

View online: https://doi.org/10.1016/S1875–5364(26)61172–7

Chinese Journal of Natural Medicines 24 (2026) 414-426

Contents lists available at ScienceDirect

Chinese Journal of Natural Medicines

journal homepage: www.cjnmcpu.com/

Original article

Targeting of MARK2, but not other MARKs, suppresses TNBC progression by inhibition of the mutant p53-driven signaling pathway

Min Zhang[a,Δ], Xilong Zhu[a,Δ], Mengqian Cui[a,Δ], Yinan Guan[b], Yong Zhang[a], Stephen J Weiss[c], Jun Chen[d], Yongzhong Yao[b,*], Rong Fu[a,*], Zhaoqiu Wu[a,*]

[a] *State Key Laboratory of Natural Medicines, Department of Pharmacology, School of Pharmacy, China Pharmaceutical University, Nanjing 211198, China*
[b] *Division of Breast Surgery, Department of General Surgery, Nanjing Drum Tower Hospital, The Affiliated Hospital of Nanjing University Medical School, Nanjing 210009, China*
[c] *The Life Sciences Institute, Department of Internal Medicine, University of Michigan Medical School, Ann Arbor 48109, USA*
[d] *Department of Pathology, Nanjing Drum Tower Hospital, The Affiliated Hospital of Nanjing University Medical School, Nanjing 210009, China*

ARTICLE INFO

Article history:
Received 16 March 2025
Revised 7 June 2025
Accepted 9 June 2025
Available online 20 April 2026

Keywords:
MARK2
mutp53
THBS1 and HBEGF
Dominant-negative MARK2
TNBC progression

ABSTRACT

Triple-negative breast cancer (TNBC) is the most challenging breast cancer subtype to treat due to the absence of effective targeted therapies. In this study, we demonstrate that elevated expression of microtubule affinity-regulating kinase 2 (*MARK2*), but not other MARK family members (*MARK1*, *MARK3*, and *MARK4*), correlates with poor prognosis in TNBC patients. Silencing *MARK2* impairs TNBC progression *via* inhibition of mutant p53 (mutp53) signaling. In contrast, silencing any of the other three MARKs either enhances or does not affect TNBC cell growth or migration and has no impact on mutp53 expression. Notably, direct knockdown of mutp53 recapitulates the effects of *MARK2* ablation in TNBC cells, further supporting a functional linkage. Moreover, ectopic expression of either wild-type (WT) *MARK2* or its kinase-dead (KD) mutant enhances mutp53 signaling and promotes TNBC progression; however, *MARK2* overexpression does not alter wild-type p53 (wtp53) expression or cell growth in luminal breast cancer cells. Significant inverse correlations are also observed between the expression levels of *MARK2*, *THBS1*, or *HBEGF* (two direct target genes of mutp53) and both overall and disease-free survival in TNBC patients harboring mut*TP53*, whereas no such association exists between *MARK2* and survival in breast cancer subtypes expressing wt*TP53*. *MARK2* is predominantly localized in the nucleus of TNBC cells, where it interacts with and stabilizes mutp53 through its UBA and Spacer domains. Consistent with this, *MARK2*-ΔUBA or *MARK2*-ΔSpacer mutant proteins fail to bind mutp53 or sustain its signaling, thereby acting as dominant-negative inhibitors that suppress TNBC progression. Collectively, our findings indicate that suppressing *MARK2* expression, rather than inhibiting its kinase activity, may represent an effective therapeutic strategy for TNBC with mut*TP53*.

1. Introduction

Breast cancer remains the most common malignancy and the second leading cause of cancer-related mortality among women worldwide [1]. Triple-negative breast cancer (TNBC) is a heterogeneous subtype characterized by the absence of estrogen receptor (ER), progesterone receptor (PR), and human epidermal growth factor receptor 2 (HER2), and accounts for approximately 15% of all breast cancer cases [2–4]. Patients with TNBC exhibit a worse prognosis than those with other subtypes (i.e., luminal and HER2$^+$ breast cancer) due to higher recurrence rates and a lack of effective targeted therapies [5]. TNBC is typically more aggressive and more prone to distant metastasis compared to other breast cancer subtypes [6]. Additionally, therapeutic resistance is frequently observed in metastatic TNBC [7]. Therefore, the discovery and validation of effective therapeutic targets for TNBC treatment are urgently needed.

The tumor suppressor protein p53, encoded by the *TP53* gene and known as the "guardian of the genome", suppresses tumorigenesis through multiple pathways [8]. The *TP53* gene is the most frequently mutated gene in human cancers, including breast cancer [9, 10]. Somatic mutations in *TP53* occur in approximately 80% of TNBC patients [11]; the resulting mutant p53 (mutp53) not only loses its tumor-suppressive functions but also acquires gain-of-function (GOF) properties that promote cell proliferation, invasion, resistance to apoptosis, and genomic instability, collectively contributing to the high aggressiveness and therapeutic resistance observed in TNBC [12–15]. Thus, mut*TP53* can be regarded as an oncogene that actively drives TNBC progression, and accumulated mutp53 represents a potential therapeutic target for mut*TP53*-bearing malignancies, including TNBC [16–19]. However, the regulatory mechanisms governing mutp53 accumulation remain incompletely understood.

Microtubule-affinity regulating kinases (MARKs, also known as PAR-1), a family of serine/threonine protein kinases, participate in diverse cellular processes, including cell polarization, cytoskeletal stability, cell-cycle regulation, and intracellular signal

* Corresponding author.
E-mail addresses: loyal1006@hotmail.com (Y. Yao); furong@cpu.edu.cn (R. Fu); zqwu@cpu.edu.cn (Z. Wu)
Δ These authors contributed equally to this work.

https://doi.org/10.1016/S1875-5364(26)61172-7

transduction [20–23]. The MARK family comprises four members (*MARK1-4*), each containing an N-terminal leader sequence, a highly conserved kinase catalytic (CA) domain, a ubiquitin-associated (UBA) domain, a spacer region, and a C-terminal kinase-associated (KA1) domain [24–26]. In contrast to the CA domain, the UBA and Spacer domains exhibit greater variability in size and sequence identity across MARK family members, which may underlie their distinct functional roles in specific disease contexts [27–30]. Nevertheless, the precise contributions of individual MARK isoforms to tumor development and progression remain unclear.

In this study, we focused on elucidating the role of *MARK2* within the MARK kinase family in triple-negative breast cancer. This focus was motivated by integrated transcriptomic and proteomic analyses of TCGA and CPTAC datasets, which revealed that *MARK2*, but not *MARK1*, *MARK3*, or *MARK4*, is significantly upregulated in TNBC and uniquely associated with poor patient survival. Given this subtype-specific enrichment and clinical relevance, we further evaluated the functional and molecular significance of *MARK2* in TNBC models. Our study aims to determine whether *MARK2* functions as a distinct tumor-promoting factor in mut*TP53*-driven TNBC, and to uncover the underlying molecular mechanisms.

2. Materials and methods

2.1. Cell culture

The SUM159 (CVCL_5590) cell line was purchased from BioIVT. MDA-MB-231 (CVCL_0062), HEK-293T (CVCL_0063), and MCF7 (CVCL_0031) cell lines were purchased from ATCC. MDA-MB-231 cells harbor a homozygous *TP53* mutation (R280K) and exclusively express mutp53. SUM159 cells carry a heterozygous mutation (Leu insertion at V157-R158), but wild-type p53 (wtp53) protein is barely detectable under basal conditions due to rapid degradation. MCF7 cells express wild-type *TP53* (wt*TP53*) and were used as a control for wtp53. Genotypes were confirmed *via* the COSMIC and ATCC databases and informed the interpretation of p53-related findings. All cell lines were cultured in DMEM supplemented with 10% FBS and 1% penicillin-streptomycin. Mycoplasma contamination was tested every two months, and only mycoplasma-negative cells were used. All cell lines in this study were authenticated in our laboratory.

2.2. Clinical data analysis

Gene expression data and corresponding clinical information for *MARK1-4*, *HBEGF*, and *THBS1* were obtained from the Assistant for Clinical Bioinformatics (ACLBI) platform (https://www.aclbi.com/static/index.html#/), which provides RNA-sequencing expression profiles and clinical correlation analyses using data from The Cancer Genome Atlas (TCGA) dataset (https://portal.gdc.cancer.gov). All statistical analyses and R packages were implemented using R software version 4.0.3 (The R Foundation for Statistical Computing, 2020). A P value < 0.05 was considered statistically significant. Kaplan-Meier survival analysis with the log-rank test was used to compare survival differences between groups. For Kaplan-Meier curves, P-values and hazard ratios (HRs) with 95% confidence interval (CI) were generated using log-rank tests and univariate Cox proportional hazards regression. Protein expression data and corresponding clinical information for *MARK1-4* were derived from the TCGA dataset (https://ualcan.path.uab.edu/index.html). UALCAN provides protein expression analysis using data from the Clinical Proteomic Tumor Analysis Consortium (CPTAC). Z-scores represent standard deviations from the median across samples for the given cancer type. Log_2 Spectral count ratio values from CPTAC were first normalized within each sample profile, then normalized across samples.

2.3. RNA-Sequencing (RNA-Seq)

Total RNA was extracted from each group (n = 3 biological replicates per group) and submitted to Novogene (Beijing, China) for transcriptome sequencing. The quantity and integrity of total RNA were assessed using the RNA Nano 6000 Assay Kit on an Agilent Bioanalyzer 2100 system (Agilent Technologies, CA, USA), with all samples exhibiting an RNA integrity number (RIN) > 7.0. Polyadenylated mRNA was purified from total RNA using Oligo (dT) magnetic beads and fragmented into short fragments using divalent cations at elevated temperatures. First-strand cDNA was synthesized using random hexamer primers and reverse transcriptase, followed by second-strand synthesis with DNA polymerase I and dNTPs. The resulting double-stranded cDNA fragments were subjected to end repair, 3′ adenylation, and ligation with looped adaptors. Library fragments of approximately 370–420 bp were size-selected and purified using the AMPure XP system (Beckman Coulter, Beverly, USA). PCR amplification was then performed, and the final libraries were purified again with AMPure XP beads. The quality and quantity of the libraries were validated, and sequencing was conducted on the Illumina NovaSeq 6000 platform to generate 150 bp paired-end reads. Raw sequencing data were processed and analyzed according to Novogene's in-house bioinformatics pipeline.

2.4. Reverse transcription-quantitative polymerase chain reaction (RT-qPCR) assay

Total RNA was isolated and reverse-transcribed into cDNA using TRIzol reagent (Invitrogen, #15596018) and PrimeScript™ RT reagent Kit (Takara, #RR047Q) according to the manufacturer's instructions. Quantitative RT-PCR was performed on an Applied Biosystems QuantStudio 3 qPCR system (Thermo Fisher Scientific), and relative mRNA expression levels were normalized to glyceraldehyde-3-phosphate dehydrogenase (*GAPDH*). Primers for the indicated genes are listed in Supplementary Table 1.

2.5. Cell proliferation assay

Cell viability was measured by CCK-8 assay (Vazyme, #A311-01) according to the manufacturer's instructions. Briefly, SUM159 and MDA-MB-231 cells were seeded in a 96-well plate at a density of 500−1000 cells per well. At the designated time point, the medium was replaced with fresh DMEM containing 10% CCK-8 reagent and incubated for 1 h. Absorbance was then measured at 450 nm using a Molecular Devices microplate reader.

2.6. Cell migration assay

Cell migration was assessed using 8-μm pore size transwell chambers (Corning, #354480) in 24-well plates. A total of 6×10^4 cells were seeded in the upper chamber with FBS-free culture medium, while the lower chamber was filled with complete medium containing 10% FBS. Cells were allowed to migrate for 10 or 13 h. Non-migrated cells on the upper surface were removed with a cotton swab, and migrated cells on the lower surface were fixed with methanol, stained with 0.3% crystal violet, and subsequently photographed and quantified.

2.7. Colony formation assay

SUM159 or MDA-MB-231 cells (500-1000 cells per well) were seeded into 6-well plates and allowed to adhere for 24 h. The medium was replaced twice per week. After 12 or 18 days of incubation, colonies were fixed with methanol, stained with 0.3%

crystal violet, and photographed and quantified.

2.8. Flow cytometric analysis

For apoptosis analysis, cells were seeded into 6-well plates and incubated for 48 h before processing according to the manufacturer's instructions. Apoptotic cell percentages were determined using the Annexin V-FITC/PI Apoptosis Detection Kit (YEASEN, #40302ES50). For cell cycle analysis, cell cycle phases were assessed using a Cell Cycle Detection Kit (Keygen Biotech, #KGA9101). Prepared cell samples were analyzed using a FACS Celesta flow cytometer (BD Biosciences). Apoptosis data were analyzed with FlowJo software, and cell cycle data were analyzed with ModFit LT software.

2.9. Cloning, lentivirus production, and cell transfection

Plasmids pLKO.1-TRC (#10879), psPAX2 (#12260), and pMD2.G (#12259) were purchased from Addgene. Plasmids pLKO.1-Neo-*TP53*-shRNA (#P33186), pLKO.1-Neo-vector (#P33186), pLenti-puro-Luciferase-GFP (#119816), pCDNA3.1-6xHis-*MARK2* (#P19259), and pCDNA3.1-*MARK3*-3xMyc (#P55459) were purchased from MiaoLing Biology. Plasmids pLenti-*MARK2*-WT-GFP, pLenti-*MARK2*-T208A/S212A, and pLKO.1-*MARK1-4*-shRNA were generated in our laboratory. Plasmids pLenti-puro-*MARK2*-ΔUBA-GFP and pLenti-puro-*MARK2*-ΔSpacer-GFP were constructed by GenScript Biotech Inc. (Nanjing, China). shRNA sequences are listed in Supplementary Table 1. To produce lentiviral particles, HEK-293T cells were co-transfected with pLKO.1-shRNA or pLenti-puro-GFP, psPAX2, and pMD2.G at a 4∶3∶1 ratio using Lipofectamine 2000 reagent (Invitrogen, #11668-019) according to the manufacturer's instructions. Fresh medium was added 24 h post-transfection, and viral particle-containing conditioned medium was harvested at 48 and 72 h. For lentiviral infection, target cells were incubated with a 1∶1 mixture of viral particles and fresh culture medium containing polybrene (8 μg·mL^{-1}; Sigma-Aldrich, #H2968) for 24 h. Cells were then incubated for an additional 24 h and selected by culturing in 0.5 μg·mL^{-1} puromycin (Sangon Biotech, #A610593) or 1.6 mg·mL^{-1} G418 (Sangon Biotech, #A100859) for 5 d before downstream applications. This selection duration was optimized based on preliminary time-course titration experiments to ensure complete elimination of uninfected cells, as confirmed by the absence of viable cells in parallel untransduced control cultures. Stable knockdown integrity was further verified by RT-qPCR before each experiment. Following the 5-day selection, cells were maintained for no more than two passages in medium supplemented with half the original concentration of puromycin or G418 to sustain selective pressure and minimize transgene loss.

2.10. Protein expression and purification

Sequences encoding full-length *MARK2* and domain-deletion variants (ΔCA), UBA domain-deleted (ΔUBA), Spacer domain-deleted (ΔSpacer), and KA1 domain-truncated (ΔKA1) were cloned into the pET-28a expression vector. Recombinant His-tagged *MARK2* proteins were purified from *E. coli* (BL21) by Ni-NTA agarose (Invitrogen, #R90101) affinity chromatography. Cells were pelleted and lysed in lysis buffer (20 mmol·L^{-1} HEPES, 500 mmol·L^{-1} NaCl, 20 mmol·L^{-1} imidazole, 10% Glycerol, pH 7.5), then eluted stepwise using 100, 300, 500 mmol·L^{-1} imidazole in wash buffer. Sequence encoding mutp53 for R280K and insert Leucine within V157-R158 were cloned into the pGEX-6P-1 expression vector. Recombinant GST-tagged p53 proteins were purified using glutathione-agarose (Thermo Fisher Scientific, #16100) affinity chromatography. Cells were pelleted and lysed in lysis buffer (20 mmol·L^{-1} HEPES, 500 mmol·L^{-1} NaCl with PH 7.5 and eluted stepwise with elution buffer containing 10 mmol·L^{-1} reduced L-glutathione (pH 7.5). Purified proteins were validated by Coomassie staining.

2.11. Immunoblot, immunoprecipitation, and GST/His pull-down

For immunoblot analysis, cells were lysed in RIPA lysis buffer (Thermo Fisher Scientific, #89900) supplemented with protease inhibitor cocktail (Selleck, #B14002). For subcellular fractionation, nuclear and cytoplasmic proteins were extracted using the NE-PER™ Nuclear and Cytoplasmic Extraction Reagent Kit (Thermo Fisher Scientific, #89900). *GAPDH* served as a loading control for cytoplasmic proteins, and *HDAC1* for nuclear proteins. Equal amounts of protein were separated by SDS-PAGE and transferred onto nitrocellulose (NC) membranes (Millipore, #HATF00010). Membranes were blocked in 5% non-fat milk in PBST for 1 h at room temperature, then incubated overnight at 4 °C with the following primary antibodies against *MARK2* (Santa Cruz Biotech, sc-47778; 1∶1000), *MARK1* (Proteintech, 21552-1AP; 1∶1000), *MARK3* (Abcam, ab52626; 1∶0000), *MARK4*(Abmart, MG288507S; 1∶1000), p53 (Santa Cruz Biotech, sc-98; 1∶1000), *THBS1* (Santa Cruz Biotech, sc-393504; 1∶1000), *β*-actin (Santa Cruz Biotech, sc-47778; 1∶1000), *GAPDH* (Santa Cruz Biotech, sc-32233; 1∶1000), Cyclin D1 (CST, #55506; 1∶1000), Ubiquitin (CST, #3933; 1∶1000), *HDAC1* (CST, #34589; 1∶1000), Myc-Tag (CST, #2276; 1∶1000), His-Tag (CST, #12698S; 1∶1000), FLAG-Tag (Sigma-Aldrich, #F3165; 1∶2000), GST-Tag (BioLegend, #640801; 1∶1000), followed by incubation with appropriate horseradish peroxidase (HRP)-conjugated secondary antibodies. Blots were visualized using enhanced chemiluminescence (Thermo Fisher Scientific, #34580). A pan-p53 antibody (Santa Cruz Biotech, sc-98) was used for p53 detection, which recognizes both mutp53 and wtp53 isoforms. Although this antibody does not distinguish between p53 isoforms at the protein level, the interpretation of results was guided by the known *TP53* genotypes of the cell lines (e.g., MDA-MB-231: homozygous mutant; SUM159: mutant-dominant; MCF7: wild-type only). For immunoprecipitation (IP), cells were lysed in IP lysis buffer (50 mmol·L^{-1} Tris-HCl, 150 mmol·L^{-1} NaCl, 1 mmol·L^{-1} EDTA, 1% NP-40, PH 7.4) containing protein inhibitor cocktail on ice. containing protease inhibitors on ice. Lysates were sonicated, clarified, and incubated with antibodies against immunoglobulin G, *MARK2* (1∶100), p53 (1∶100), or Myc-tag (1∶250), followed by incubation with pre-cleared protein A/G agarose beads (Santa Cruz Biotech, #sc-2003). Immune complexes were analyzed by immunoblotting. For pull-down assays, His- or GST-tagged recombinant proteins were expressed and purified from *E. coli* (BL21). GST-tagged protein mixtures were preincubated overnight at 4 °C on a rotator; glutathione-agarose beads were then added for 2 h. Beads were collected, washed, electrophoresed, and subjected to Coomassie staining. In additional experiments, various His-tagged *MARK2* recombinant proteins were immobilized on Ni-NTA agarose and incubated overnight at 4 °C with SUM159 whole-cell lysates. Bound protein complexes were washed, eluted in SDS loading buffer, resolved by SDS-PAGE, and analyzed by immunoblotting.

2.12. Immunocytochemistry and immunohistochemistry

For immunohistochemistry, cells were cultured on coverslips in 24-well plates for 48 h, washed twice with PBS, fixed with 4% paraformaldehyde (PFA) for 10 min, permeabilized with 1% Triton X-100 in PBS for 30 min, and blocked with blocking buffer (0.5% BSA and 5% goat serum in PBS) for 30 min. The cells were then incubated overnight at 4 °C with the indicated primary antibodies against *MARK2* (Sigma-Aldrich, #HPA074905; 1∶300), p53 (CST, #2527, 1∶100), GFP (Invitrogen, a10262; 1∶100)

overnight at 4 °C, followed by incubation with goat anti-Rabbit or anti-Chicken Alexa secondary antibodies (all from Thermo Fisher Scientific). The cells were subsequently counterstained with DAPI (Thermo Fisher Scientific, #D1306) and imaged using a Zeiss LSM800 microscope. For immunohistochemistry, paraffin-embedded tumor tissues were sectioned at 5 μm, deparaffinized in three changes of xylene, and rehydrated through a graded ethanol series. For antigen retrieval, the slides were heated in citric acid-based Antigen Unmasking Solution (#H-3300, Vector Laboratories), allowed to cool naturally to room temperature, and permeabilized with 0.3% Triton X-100 in PBS for 30 min. Endogenous peroxidase activity was blocked with 1% H_2O_2 for 30 min. The slides were then blocked with blocking buffer for 40 min and incubated overnight at 4 °C with the indicated primary antibodies against Ki-67 (Abcam, ab15580; 1∶2000), phospho-histone H3 (CST, #9701; 1∶200), cleaved caspase 3 (CST, #9661; 1∶400), cyclin D1 (CST, #55506; 1∶300), p53 (CST, #2527; 1∶100), and THBS1 (Abcam; ab267388; 1∶5000). The sections were subsequently incubated with biotin-labeled goat anti-mouse or goat anti-rabbit IgG secondary antibodies for 1 h, followed by avidin–biotin complex (#PK-6101, Vector Laboratories). DAB chromogen (#SK-4105, Vector Laboratories) was used for color development. Finally, all slides were counterstained with hematoxylin and mounted with neutral resin.

2.13. Tumor xenograft model and human tumor samples

Mice were housed under standard specific pathogen-free (SPF) conditions, and all animal experiments were performed in accordance with protocols approved by the Animal Welfare and Ethics Committee of China Pharmaceutical University. Female BALB/c nude mice aged from 6–8 weeks were purchased from Shanghai Model Organisms Center, Inc (Shanghai, China). A single-cell suspension of 2×10^6 MDA-MB-231 cells in a total volume of 100 μL of PBS diluted with Matrigel (1∶1, Corning; #354262) was injected subcutaneously into the dorsal flank of each mouse. Mice were randomized into three groups prior to inoculation. Tumor volumes were measured every other day using the formula ($\pi \times$ length $\times$ width^2/6). At the predetermined endpoint, mice were euthanized, and tumors were dissected, photographed, and weighed. Tissues were either fixed in 4% paraformaldehyde (PFA) for immunohistochemical analysis or snap-frozen in liquid nitrogen and stored at −80 °C for immunoblot analysis. Human TNBC tumor and paired normal tissues were provided by Nanjing Drum Tower Hospital (Nanjing, China) and stored at −80 °C. The use of human materials was approved by the Ethics Committee of Nanjing Drum Tower Hospital, the Affiliated Hospital of Nanjing University Medical School, with informed consent obtained from all patients.

2.14. Statistical analysis

Data were presented as mean ± SD. Statistical analyses were performed using GraphPad Prism (version 9.0) and *R* (version 4.0.3), as appropriate. For comparisons between two independent groups (e.g., TNBC tumors *vs* matched normal tissues), a two-tailed unpaired Student's *t*-test was used, consistent with standard practice for transcriptomic and proteomic datasets with assumed normal distribution (e.g., TCGA and CPTAC). For freshly dissected TNBC tumors and matched adjacent normal tissues, the two-tailed paired Student's *t*-test was employed. For comparisons among more than two groups, one-way ANOVA followed by Dunnett's multiple comparisons test was applied. For longitudinal tumor volume measurements, repeated-measures models (linear mixed-effects) were employed. For survival analysis, Kaplan–Meier curves with log-rank test and univariate Cox proportional hazards regression were used. The specific statistical method used is indicated in each figure legend. *P*-value < 0.05 was considered statistically significant.

2.15. Data availability

The RNA-seq data generated in this study are publicly available in BioProject database at PRJNA1202101.

3. Results

3.1. Increased expression of *MARK2*, but not the other three MARK family members, worsens survival rates of TNBC patients

Using the ACLBI (The Assistant for Clinical Bioinformatics Portal) online tool, we analyzed the dataset from TCGA to determine the relationship between expression levels of individual *MARK* genes and clinical outcomes across the three major molecular subtypes of breast cancer (i.e., luminal, HER2$^+$, and triple-negative subtypes). No statistically significant associations were observed between *MARK1*, *MARK3*, or *MARK4* expression and overall survival (OS) or disease-free survival (DFS) in any of the three subtypes (Fig. 1A and Supplementary Figs. S1A and S1B). Nevertheless, *MARK1*-high tumors exhibited a trend toward better prognosis in the TNBC subtype, reflected by a slight, albeit non-significant, increase in OS (Fig. 1A). Of note, a significant inverse association was identified between *MARK2* expression and both OS and DFS specifically in the triple-negative subtype, but not in luminal or HER2$^+$ breast cancer subtypes (Fig. 1B). Additionally, we used ACLBI and UALCAN (The University of Alabama at Birmingham Cancer Data Analysis Portal) to analyze MARK expression at the transcript and protein levels in TNBC tumors versus matched normal tissues. As expected, both mRNA and protein levels of *MARK1* were lower in TNBC tumors than in matched normal tissues, whereas *MARK2* levels were robustly elevated in TNBC tumors (Figs. 1C and 1D). No obvious difference in mRNA or protein expression levels of *MARK3* in TNBC tumors versus matched normal tissues was identified (Figs. 1C and 1D). No substantial differences in *MARK3* mRNA or protein expression were detected between TNBC tumors and matched normal tissues (Figs. 1C and 1D). To further clarify the expression pattern of *MARK2* in TNBC subtypes, the freshly-dissected tumors and matched normal tissues were collected from TNBC patients and subjected to RT-qPCR and immunoblotting analyses. Consistent with *MARK2* expression pattern identified in the datasets, TNBC tumors indeed exhibited remarkably increased expression of *MARK2* at both the mRNA and protein levels compared to matched normal tissues (Figs. 1E and 1F). Collectively, these findings indicate that *MARK2*, but not the other three MARK family members, may serve as a potential marker of poor prognosis in TNBC.

3.2. Silencing of *MARK2*, but not the other three MARK family members, impairs TNBC tumor progression

To directly test the putative tumor-promoting or tumor-suppressive functions of individual MARKs, we used shRNA-expressing lentiviral vectors to stably silence expression of each MARK in human TNBC cell lines MDA-MB-231 and SUM159. RT-qPCR and immunoblotting analyses confirmed remarkably decreased levels of individual MARKs in TNBC cells that stably expressed corresponding lentiviral shMARK vectors (Figs. 2A and 2C and Supplementary Figs. S2A and S2C). Cell proliferation was assessed using the Cell Counting Kit-8 (CCK-8) and colony formation assays. As anticipated, silencing *MARK3* or *MARK4* had minimal effects on the growth of MDA-MB-231 and SUM159 cells (Figs. 2B and 2D and Supplementary Figs. S2B and S2D). Intriguingly, *MARK1* si-

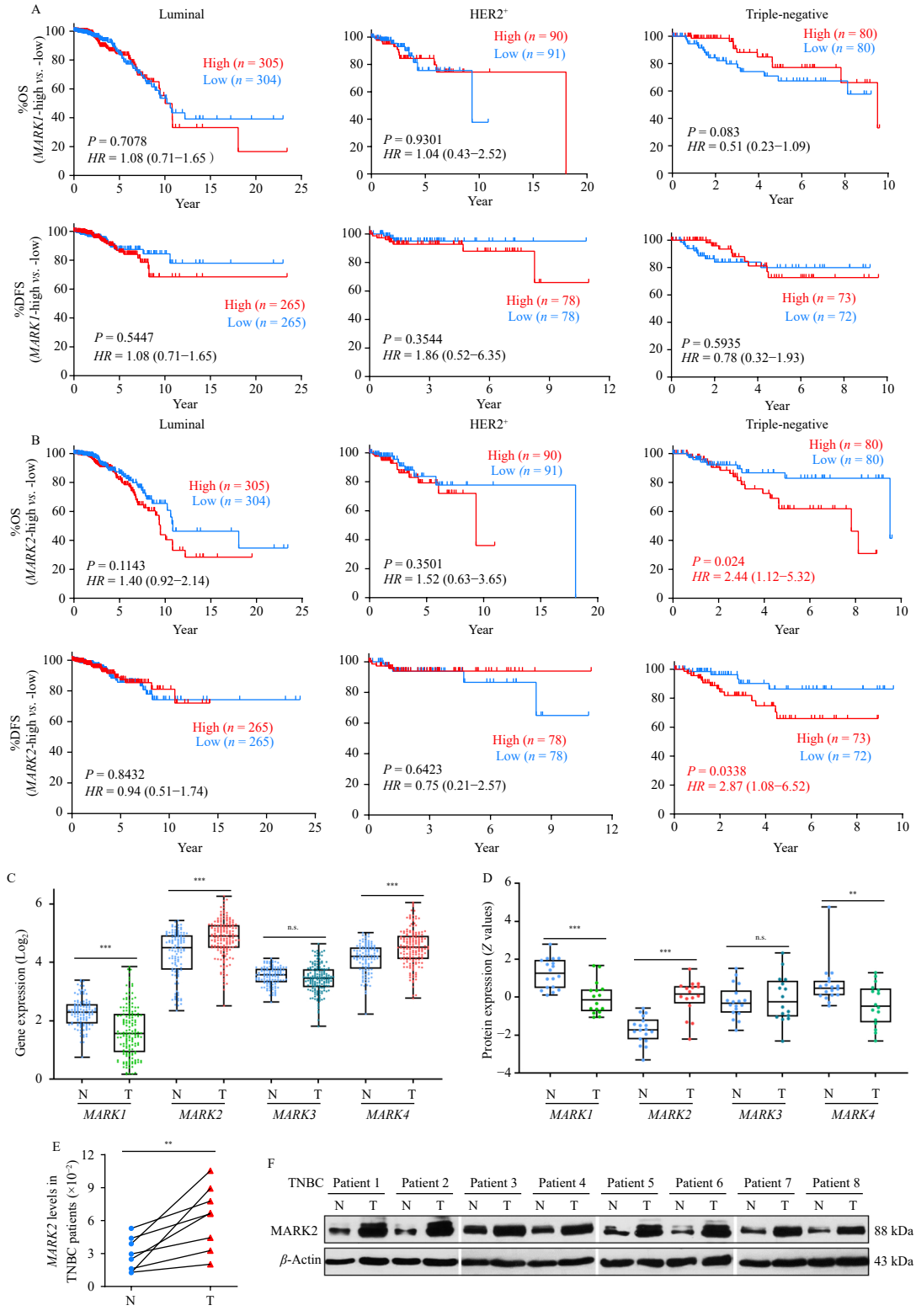

Fig. 1 Increased expression of *MARK2* is correlated with poor prognosis in TNBC. (A, B) Kaplan–Meier curves for overall survival (OS) and disease-free survival (DFS) in luminal, HER2$^+$, and triple-negative breast cancer (TNBC) subtypes, stratified by high and low expression of *MARK1* (A) or *MARK2* (B). Survival data were obtained from the TCGA database and analyzed using the log-rank (Mantel-Cox) test. Hazard ratios (HRs) and 95% confidence intervals (CIs) were calculated using univariate Cox proportional hazards regression. (C, D) Relative mRNA (C) and protein (D) expression levels of *MARK1*–*MARK4* in TNBC tumor tissues (T) and non-paired normal breast tissues (N), based on the TCGA and CPTAC datasets, respectively. Data are presented asmeans ± SD. Statistical significance was assessed using a two-tailed unpaired Student's *t*-test. (E, F) RT-qPCR (E) and immunoblotting (F) analyses of MARK2 expression in freshly dissected TNBC tumors (T) and matched adjacent normal tissues (N) from the same patients. Statistical significance in (E) was assessed using a two-tailed paired Student's *t*-test. $^{**}P < 0.01$, $^{***}P < 0.001$; n.s., not significant.

lencing robustly enhanced the growth of MDA-MB-231 cells, confirming the tumor growth-suppressive function of *MARK1* in TNBC cells (Figs. 2B and 2E and Supplementary Fig. S2B). By contrast, silencing expression of *MARK2* remarkably suppressed the growth of MDA-MB-231 and SUM159 cells, confirming the tumor growth-promoting function of *MARK2* in TNBC cells (Figs. 2B, 2D and 2E and Supplementary Figs. S2B and S2D). Notably, only *MARK2* silencing, and not that of the other three MARK family members, effectively inhibited the migratory capacity of TNBC cells (Supplementary Figs. S2E and S2F). Annexin V/PI dual stain-

ing assay revealed that *MARK2* silencing failed to induce cell apoptosis, suggesting that genetic inhibition of *MARK2* has no impact on the survival of MDA-MB-231 and SUM159 cells (Supplementary Figs. S2G and S2H). We therefore investigated whether *MARK2* inhibition influences cell cycle progression. Control and *MARK2*-silenced TNBC cells were treated with vehicle or the microtubule-destabilizing agent nocodazole for 12 h and subjected to FACS analysis. A subtle but significant G1 phase arrest was observed in vehicle-treated, *MARK2*-silenced MDA-MB-231 and SUM159 cells (Supplementary Figs. S2I and S2J). Following 12 h of nocodazole treatment, a large fraction of control cells accumulated in the G_2/M phase, whereas most *MARK2*-silenced cells remained in the G_1 phase, with a substantially smaller fraction progressing to the G_2/M phase (Supplementary Figs. S2I and S2J).

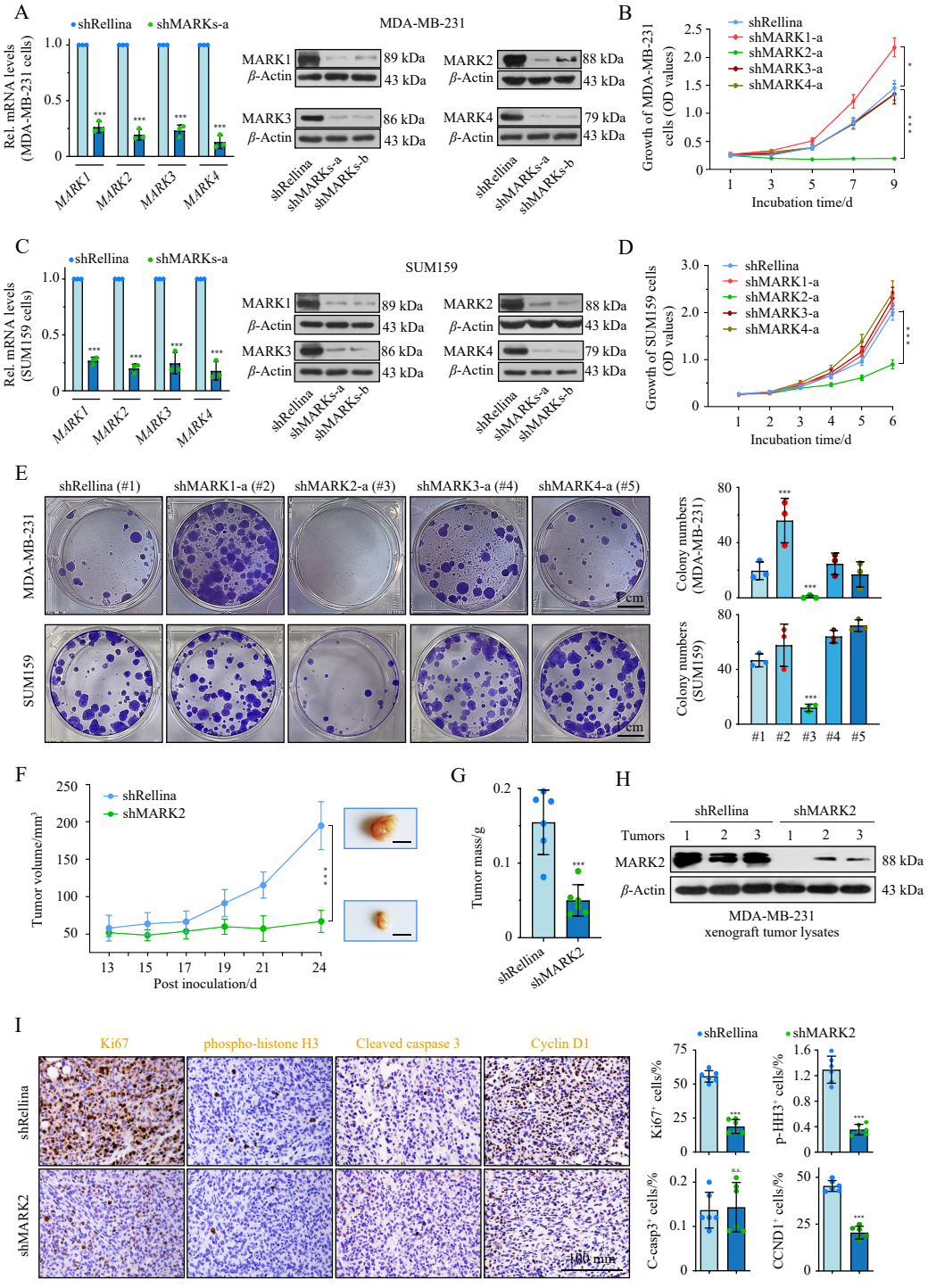

Fig. 2 Silencing *MARK2*, but not *MARK1*, *MARK3*, or *MARK4*, impairs TNBC progression. (A, C) RT-qPCR and immunoblotting analyses showing the efficiency of stable knockdown of *MARK1*–*MARK4* in MDA-MB-231 (A) and SUM159 (C) cells using lentiviral shRNA vectors. MDA-MB-231 cells harbor the *TP53* R280K mutation, whereas SUM159 cells harbor the *TP53* V157-R158insL mutation. (B, D) Cell proliferation curves assessed by CCK-8 assay in MDA-MB-231 (B) and SUM159 (D) cells following stable knockdown of *MARK1*–*MARK4*. Cell growth was monitored over time. (E) Colony formation assays evaluating the clonogenic potential of MDA-MB-231 and SUM159 cells after silencing of each MARK isoform. (F, G) Tumor growth curves measured every day (F) and final tumor weights (G) of xenograft tumors derived from shRenilla control or sh*MARK2* MDA-MB-231 cells following subcutaneous inoculation into nude mice. (H) Immunoblotting analysis confirming reduced *MARK2* protein levels in xenograft tumor lysates. (I) Immunohistochemical staining and quantification of Ki-67, phospho-histone H3, cleaved caspase-3, and cyclin D1 in xenograft tumor sections. Approximately 1,000 cells were counted across 10 random microscopic fields per section. Data are presented as mean ± SD. n = 3 biological replicates for *in vitro* assays; n = 6 mice per group for *in vivo* experiments. Statistical analyses were performed using: two-tailed unpaired Student's t-test (A, C, G, I), one-way ANOVA with Dunnett's test (E), longitudinal models for time-course proliferation and tumor growth data (B, D, F). $^{*}P < 0.05$, $^{***}P < 0.001$; n.s., not significant.

These observations indicate that *MARK2* silencing causes a pronounced defect in the transition from G_1 to S phase, a critical cell cycle checkpoint essential for tumor cell proliferation [31].

We next assessed the impact of *MARK2* silencing on TNBC cell growth *in vivo*. Control and *MARK2*-silenced MDA-MB-231 cells were inoculated into nude mice, and xenograft tumor growth was monitored over 24 days. Consistent with the *in vitro* studies, *MARK2* silencing suppressed xenograft tumor growth, as evidenced by significant reductions in tumor size and mass (Figs. 2F and 2G). Immunoblotting of tumor lysates confirmed markedly reduced *MARK2* expression in xenografts derived from *MARK2*-silenced cells compared to controls (Fig. 2H). Consistently, immunohistochemical staining of *MARK2*-silenced versus control xenograft tumors revealed markedly decreased percentages of proliferative cells ($Ki67^+$), mitotic cells (phospho-histone $H3^+$), and cyclin $D1^+$ cells (cyclin D1, a driving molecule for the G_1/S phase transition [31–33], accompanied with comparable numbers of apoptotic cells (cleaved caspase 3^+) (Figs. 2I). Taken together, these findings demonstrate that silencing *MARK2*, but not the other three MARK family members, effectively impairs TNBC tumor progression.

3.3. Silencing of *MARK2* expression represses mutp53 signaling pathway in TNBC cells

To elucidate the mechanism by which *MARK2* silencing impairs TNBC progression, we performed RNA sequencing (RNA-seq) on *MARK2*-silenced versus control MDA-MB-231 cells. Using a minimum 1.5-fold change cutoff, *MARK2* silencing altered the expression of nearly 400 unique transcripts (236 upregulated and 156 downregulated; Fig. 3A). Gene set enrichment analysis (GSEA) revealed that *MARK2* silencing affected signature genes enriched in mutp53 signaling, as well as several other oncogenic and tumor-suppressive signaling pathways, such as Notch, TGFβ, AMPK, Hippo, Insulin, and Wnt (Figs. 3B and 3C). *TP53* mutations are present in approximately 80% of TNBC cases. The resulting mutp53 gain-of-function promotes, rather than inhibits, tumor progression and has been reported to crosstalk with and regulate the aforementioned signaling pathways at multiple levels [11, 12, 34–37]. We therefore reasoned that silencing *MARK2* might impair TNBC progression through repression of the mutp53 signaling pathway. RT-qPCR analysis demonstrated that silencing *MARK2* in MDA-MB-231 cells harboring mutp53-R280K had little effect on *TP53* expression itself, but markedly regulated the expression of mutp53 target genes including *THBS1*, *HBEGF*, *EDN2*, *S1PR1* (the transcriptionally activated genes), and *CD82* and *BHLHE41* (the transcriptionally repressed genes) [38–40] (Fig. 3D). Immunoblotting analysis further confirmed that silencing *MARK2*, but not other three MARKs, robustly decreased expression levels of mutp53 and *THBS1* in MDA-MB-231 and SUM159 cells harboring mut*TP53* (Fig. 3E and Supplementary Fig. S3A). Furthermore, *MARK2*-silenced MDA-MB-231 xenograft tumors

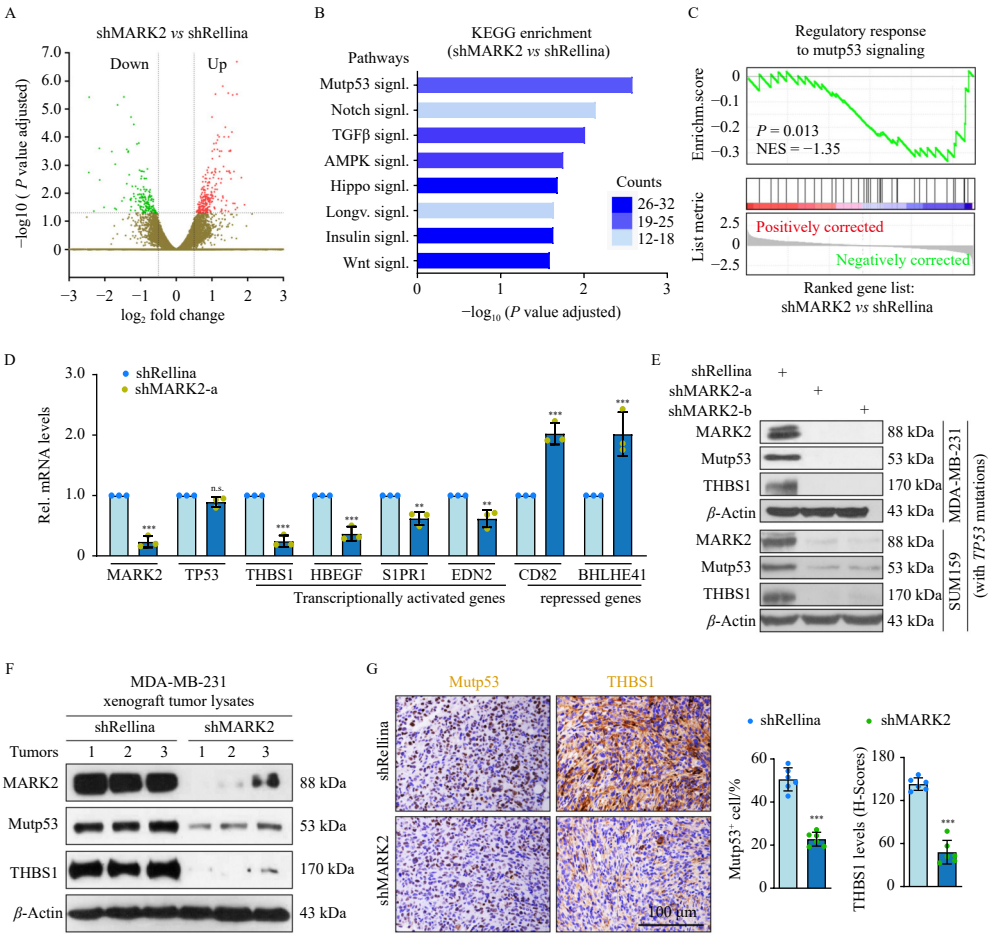

Fig. 3 Silencing of *MARK2* inhibits the mutp53 signaling pathway in TNBC cells. (A) Volcano plot of differentially expressed genes (DEGs) identified by RNA sequencing of MDA-MB-231 cells stably expressing control or *MARK2* -targeting shRNA. A 1.5-fold change and $P < 0.05$ were used as the thresholds for significant DEGs; $n = 3$ biological replicates per group. (B, C) KEGG pathway enrichment analysis (B) and gene set enrichment analysis (GSEA) (C) showing significant suppression of mutp53 signaling and several other oncogenic and tumor-suppressive pathways. (D) RT-qPCR validation of differentially expressed genes in *MARK2*-silenced and control MDA-MB-231 cells. (E) Immunoblotting analysis of *MARK2*, mutp53, and *THBS1* protein expression in *MARK2*-silenced and control MDA-MB-231 and SUM159 cells. (F, G) Immunoblotting (F) and immunohistochemical analysis (G) of *MARK2*, mutp53, and *THBS1* expression in xenograft tumors derived from control and *MARK2*-silenced MDA-MB-231 cells ($n = 6$ mice per group). Data are presented as mean ± SD. $n = 3$ biological replicates for in vitro assays; $n = 6$ mice per group for *in vivo* studies. Statistical significance was assessed using a two-tailed unpaired Student's *t*-test for (D) and (G). $^*P < 0.05$, $^{**}P < 0.01$, $^{***}P < 0.001$; n.s., not significant.

robustly decreased protein levels of mutp53 and *THBS1*, as assessed by immunoblotting and immunohistochemical analyses (Figs. 3F and 3G). RT-qPCR analysis revealed that *MARK2*-silenced xenograft tumors significantly reduced mRNA levels of *THBS1* and *HBEGF* but increased levels of *CD82*, without affecting expression of *TP53* (Supplementary Fig. S3B). Notably, RT-qPCR cannot discriminate between mutant and wild-type *TP53* transcripts because it lacks allele specificity. Therefore, mutp53 activity was inferred based on the known genotypes of the cell lines and the expression of canonical mutp53 target genes, including *THBS1* and *HBEGF*. These findings indicate that *MARK2* silencing in TNBC cells harboring *TP53* mutations reduces mutp53 protein expression and consequently represses mutp53 signaling.

3.4. Direct silencing of mutp53 expression phenocopies MARK2 abrogation in TNBC cells

We next directly assessed the impact of mutp53 silencing on TNBC cell growth and migration. As expected, mutp53-silenced MDA-MB-231 and SUM159 cells exhibited markedly reduced expression of transcriptionally activated genes (*THBS1*, *HBEGF*, *S1PR1*, and *EDN2*) in tandem with increased levels of transcriptionally repressed genes (*CD82* and *BHLHE41*), phenocopying the results observed in *MARK2*-silenced TNBC cells (Supplementary Figs. S4A and S4B). The growth and migration potentials of MDA-MB-231 and SUM159 cells were effectively reduced following mutp53 silencing, as assessed by colony formation and cell migration analyses (Supplementary Figs. S4C and S4D). Annexin V/PI dual staining assay revealed that silencing of mutp53 expression failed to induce cell apoptosis, suggesting that genetic inhibition of mutp53 has no impact on the survival of MDA-MB-231 and SUM159 cells (Supplementary Figs. S4E and S4F). We then examined cell cycle progression: control and mutp53-silenced TNBC cells were treated with vehicle or nocodazole for 12 or 15 h and analyzed by FACS. After nocodazole treatment, most control cells accumulated in G_2/M phase, whereas a large fraction of mutp53-silenced cells remained arrested in G_1 phase (Supplementary Fig. S4G). Collectively, these results demonstrate that direct mutp53 silencing phenocopies the effects of MARK2 abrogation in TNBC cells.

3.5. Ectopic expression of MARK2 promotes TNBC cell growth independently of its kinase activity, and enhanced MARK2/mutp53 signaling worsens survival in TNBC patients harboring TP53 mutations

Given that *MARK2* silencing reduces mutp53 signaling, we investigated whether *MARK2* overexpression enhances this pathway. Immunoblotting and RT-qPCR showed that *MARK2* overexpression in MDA-MB-231 and SUM159 cells substantially increased mutp53, *THBS1*, and *HBEGF* at the protein and/or mRNA levels while decreasing *CD82* expression (Figs. 4A and 4B). In contrast, *MARK2* overexpression had no significant effect on wtp53 in untreated or MG132-treated MCF7 luminal breast cancer cells (Supplementary Fig. S5A), and it did not alter MCF7 cell growth (Supplementary Fig. S5B). Next, we sought to determine whether mutp53 signaling is actively involved in the regulation of *MARK2* on TNBC cell behaviors. As shown, the increase in protein expression levels of mutp53 and THBS1 in *MARK2* overexpressed-SUM159 cells was completely abolished following the silencing of mutp53 (Fig. 4C). CCK-8 assay revealed that overexpressing *MARK2* remarkably increased the growth of SUM159 cells, and this effect was effectively reversed by concurrent silencing of (Fig. 4D). Notably, the *MARK2*/sh*TP53* group exhibited significant lower viability than the Luci/shRellina control. This finding is consistent with the near-complete loss of mutp53 protein in this group (Fig. 4C), which disables the mutp53's oncogenic support required for *MARK2*'s pro-survival effect. These results suggest that *MARK2*/mutp53 signaling pathway plays an essential role in promoting the growth of TNBC cells. We then examined whether *MARK2*-mediated upregulation of mutp53 signaling depends on its catalytic activity. Immunoblotting analysis showed that overexpression of either WT *MARK2* or the kinase-dead (KD, T208A/S212A) mutant [26] robustly increased expression levels of mutp53 and *THBS1* in SUM159 cells in a comparable fashion (Fig. 4E). Consistently, overexpression of either MARK2-WT or MARK2-KD markedly promoted SUM159 cell growth, as determined by CCK-8 assay (Fig. 4F), suggesting that *MARK2* enhances mutp53 signaling and promotes TNBC cell growth independently of its kinase activity.

Having confirmed the essential role of *MARK2*/mutp53 signaling in maintaining the malignancy of TNBC cells, we extended our experimental observations to the clinic. When examining relationships between *MARK2*, *THBS1*, and *HBEGF* mRNA levels and disease outcomes in TNBC patients, we noted significant inverse relationships between *MARK2*, *THBS1*, and *HBEGF* levels and OS as well as DFS in the patient cohort expressing mut*TP53* (Fig. 4G). Intriguingly, the relationship between *MARK2* levels and OS or DFS was absent in all subtypes of breast cancer patients expressing wt*TP53* (Supplementary Fig. S5C). These results suggest that increased *MARK2* expression or enhanced *MARK2*/mutp53 signaling worsens survival rates in TNBC patients in a *TP53* mutation-dependent fashion.

3.6. MARK2 interacts with and stabilizes mutp53 protein in TNBC cells

Given that *MARK2* regulates mutp53 expression in TNBC cells only at the protein level, we deduced that *MARK2* might interact with and stabilize mutp53. Immunofluorescence analysis illustrated that endogenous *MARK2* is primarily expressed in the nucleus of MDA-MB-231 and SUM159 cells, where it colocalizes with mutp53 (Fig. 5A). Subcellular fractionation followed by immunoblotting confirmed *MARK2* expression in both cytoplasmic and nuclear compartments, with significantly higher levels in the nucleus, where mutp53 is exclusively expressed (Supplementary Fig. S6A). Of note, both *MARK1* and *MARK3* were detected only in the cytoplasm (Supplementary Fig. S6A). To determine the putative binding interaction between *MARK2* and mutp53, we performed co-immunoprecipitation (Co-IP) analysis in MDA-MB-231 cells. A robust binding interaction between endogenously expressed *MARK2* and mutp53 was detected in the cells (Fig. 5B). As expected, epitope-tagged *MARK1* or *MARK3* failed to bind to mutp53 in MDA-MB-231 cells (Supplementary Figs. S6B and S6C), possibly resulting in their inability to effectively regulate mutp53 protein expression. To further determine whether *MARK2* could bind to mutp53 directly, we performed an *in vitro* GST pull-down assay with purified bacterially-expressed His-tagged *MARK2* and two GST-tagged mutp53 proteins (R280K as well as Leu insertion within V157-R158). We observed a direct binding interaction between *MARK2* and both mutp53 proteins (Fig. 5C). In His pull-down studies using purified bacterially expressed epitope-tagged *MARK2* or *MARK2*-deletion mutants and mutp53, UBA domain-deleted *MARK2* (*MARK2*-ΔUBA) and Spacer domain-deleted *MARK2* (*MARK2*-ΔSpacer) completely lost their ability to bind mutp53 (Figs. 5D and 5E), suggesting that both the UBA and Spacer domains are responsible for the binding interaction with mutp53. Intriguingly, an alignment analysis of amino acid identities across the four MARKs showed that *MARK2* exhibited the lowest sequence identity within the UBA and Spacer domains compared with the other three MARKs, whereas the catalytic domain displayed more than 90% identity across all four proteins (Supplementary Figs. S6D and S6E). Having established both the physical interaction between *MARK2* and mutp53 and the positive regulation of mutp53 protein expression in *MARK2*-manipulated TN-

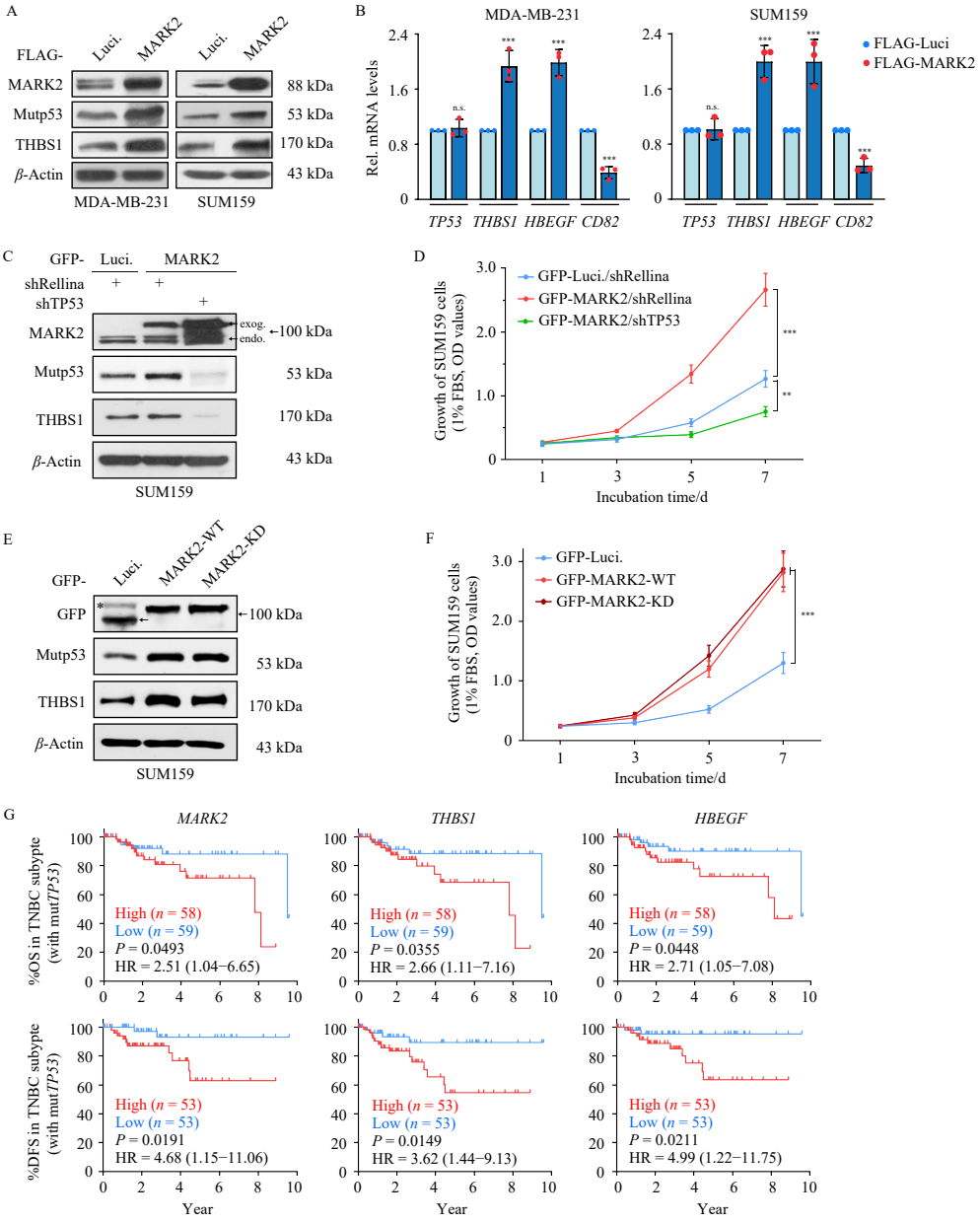

Fig. 4 Ectopic expression of wild-type *MARK2* or a kinase-dead mutant promotes TNBC progression, and enhanced *MARK2*/mutp53 signaling worsens survival in TNBC patients harboring *TP53* mutations. (A, B) Immunoblotting (A) and RT-qPCR (B) analyses of *MARK2*, mutp53, *THBS1*, and *CD82* expression in MDA-MB-231 and SUM159 cells stably expressing FLAG-tagged MARK2 or a luciferase (Luci.) control lentiviral vector. (C, D) Immunoblotting analysis of the indicated proteins (C) and CCK-8 assay for cell growth (D) in SUM159 cells first infected with GFP-tagged luciferase control or MARK2 lentiviral vectors, followed by a second infection with shRenilla control or sh*TP53* lentiviral vectors. (E, F) Immunoblotting analysis of the indicated proteins (E) and CCK-8 assay for cell growth (F) in SUM159 cells stably expressing GFP-tagged wild-type *MARK2* (WT), kinase-dead *MARK2* mutant (KD), or luciferase control lentiviral vectors. Arrows and asterisks indicate specific and nonspecific bands, respectively. (G) Kaplan–Meier analyses of overall survival (OS) and disease-free survival (DFS) in TNBC patients harboring *TP53* mutations, stratified by high and low expression of *MARK2* (left), *THBS1* (middle), or *HBEGF* (right). Patient data were obtained from the TCGA database. Comparisons were performed using the log-rank test, and hazard ratios (HRs) with 95% confidence intervals (CIs) were calculated using univariate Cox regression. Data are presented as mean ± SD. n = 3 biological replicates. Statistical analysis was performed using a two-tailed unpaired Student's t-test for mRNA comparison (B), longitudinal models for proliferation assays (D, F), and the log-rank test together with univariate Cox regression for survival analysis (G). $^{**}P < 0.01$, $^{***}P < 0.001$; n.s. refers to not significant.

BC cells, we next investigated whether *MARK2* could affect the stability of mutp53 protein. To this end, *MARK2*-silenced or control MDA-MBA-231 cells were treated with cycloheximide (CHX) for different times and subjected to immunoblotting analysis using antibodies against *MARK2* and mutp53. CHX chase analysis showed that the half-life of mutp53 protein was markedly shortened in *MARK2*-silenced cells compared to control cells (about 1.8 h *vs* about 4.0 h in $t_{1/2}$) (Fig. 5F), suggesting that silencing of *MARK2* expression destabilizes mutp53 protein in TNBC cells. Concurrently, an obvious increase in the ubiquitination levels of mutp53 was readily detected in *MARK2*-silenced MDA-MB-231 cells with robustly reduced levels of mutp53 protein (Fig. 5G).

3.7. MARK2-ΔUBA and MARK2-ΔSpacer mutants reduce TNBC cell growth by repressing the mutp53 signaling pathway, functioning as potent dominant-negative inhibitors of MARK2

Having confirmed the inability of *MARK2*-ΔUBA and *MARK2*-ΔSpacer mutants to bind mutp53 in TNBC cells, we attempted to compare the impacts of the two mutants versus *MARK2*-WT on mutp53 signaling and, subsequently, on TNBC cell growth. As predicted, expression of epitope-tagged *MARK2*-WT in SUM159 cells substantially increased expression of mutp53, *THBS1*, and *HBEGF* at the protein and (or) mRNA levels while reducing the levels of *CD82* (Figs. 6A and 6B). In striking contrast, overexpressing either *MARK2*-ΔUBA or *MARK2*-ΔSpacer mutant that is

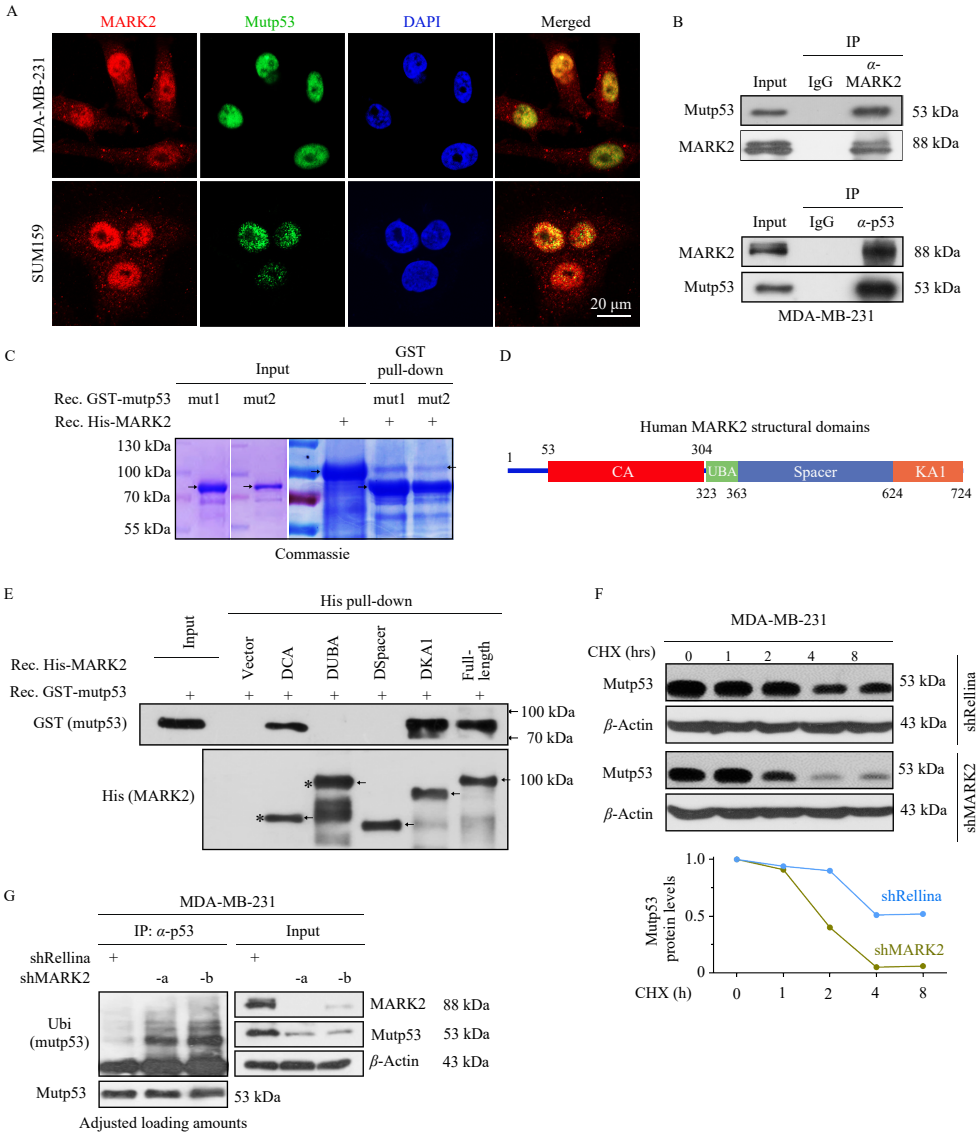

Fig. 5 *MARK2* interacts with and stabilizes mutp53 protein in TNBC cells. (A) Immunofluorescence analysis of *MARK2* and mutp53 expression and subcellular localization in MDA-MB-231 and SUM159 cells (n = 3 biological replicates per group). Nuclei were counterstained with DAPI. (B) Co-immunoprecipitation (Co-IP) assay assessing the interaction between endogenous *MARK2* and mutp53 in MDA-MB-231 cells. (C) In vitro GST pull-down assay examining the interaction between purified bacterially expressed His-tagged *MARK2* and two GST-tagged mutp53 proteins (mut1, R280K mutant; mut2, V157-R158insL mutant). (D) Schematic illustration of the structural domains of human *MARK2*. CA, catalytic domain; UBA, ubiquitin-associated domain; KA1, kinase-associated 1 domain. (E) *In vitro* His pull-down assay to determine the *MARK2* domain(s) responsible for binding mutp53 (R280K). (F) Cycloheximide (CHX; 100 μg/mL) chase analysis of mutp53 protein levels in *MARK2*-silenced and control MDA-MB-231 cells. Quantification of mutp53 levels is shown in the lower panels (n = 3 biological replicates per group). (G) Ubiquitination assay of endogenous mutp53 in *MARK2* -silenced and control MDA-MB-231 cells (n = 3 biological replicates per group). MG132 (10 μmol·L^{-1}) was added 4 h before cell harvest.

incapable of binding to mutp53 in SUM159 and MDA-MB-231 cells led to remarkably reduced, rather than increased, expression levels of mutp53, *THBS1*, and *HBEGF* in tandem with increased levels of *CD82* (Figs. 6A and 6B). This finding suggests that expression of the two *MARK2*-deletion mutants could effectively repress the mutp53 signaling pathway in TNBC cells, probably functioning as putative dominant-negative inhibitors of *MARK2*. Next, we explored the dominant-negative effect of the two *MARK2*-deletion mutants on TNBC cell growth. The CCK-8 and colony formation assays revealed that expression of either *MARK2*-ΔUBA or *MARK2*-ΔSpacer mutant significantly reduced the growth of SUM159 and MDA-MB-231 cells (Figs. 6C and 6D). To further confirm the dominant-negative effect *in vivo*, MDA-MB-231 cells were transduced with *MARK2*-ΔUBA or *MARK2*-ΔSpacer mutant and subjected to xenograft tumor growth assay. Consistent with the *in vitro* studies, *MARK2*-ΔUBA or *MARK2*-ΔSpacer mutant-transduced tumor cells exhibited robustly reduced growth rates during the 26-day period, as evidenced by significant decreases in xenograft tumor size and mass (Figs. 6E and 6F). RT-qPCR analysis revealed that *MARK2*-ΔUBA- or *MARK2*-ΔSpacer-transduced xenograft tumors significantly reduced mRNA levels of *THBS1* and *HBEGF* but increased levels of *CD82*, without affecting expression of *TP53* (Fig. 6G). Compared to Luci.-transduced xenograft tumors, *MARK2*-ΔUBA- or *MARK2*-ΔSpacer-transduced tumors displayed robustly decreased protein levels of mutp53 and *THBS1*, as assessed by immunoblotting analysis (Fig. 6H). To further confirm the functional role of UBA and Spacer domains in mutp53 stabilization, we performed CHX chase assays in cells overexpressing *MARK2*-ΔUBA or ΔSpacer. Both mutants failed to maintain mutp53 stability (Fig. 6I), with degradation kinetics similar to those in *MARK2*-knockdown cells (Fig. 5F). These results, together with prior Co-IP and ubiquitination data (Figs. 5D–5G), support that *MARK2* stabilizes mutp53 by directly binding *via* its UBA and Spacer domains to block ubiquitin-mediated degradation. Collectively, these findings demonstrate that *MARK2*-ΔUBA and *MARK2*-ΔSpacer mutants effectively reduce TNBC cell growth *in vitro* and *in vivo* by repressing mutp53 signaling pathway, functioning as potent dominant-negative inhibit-

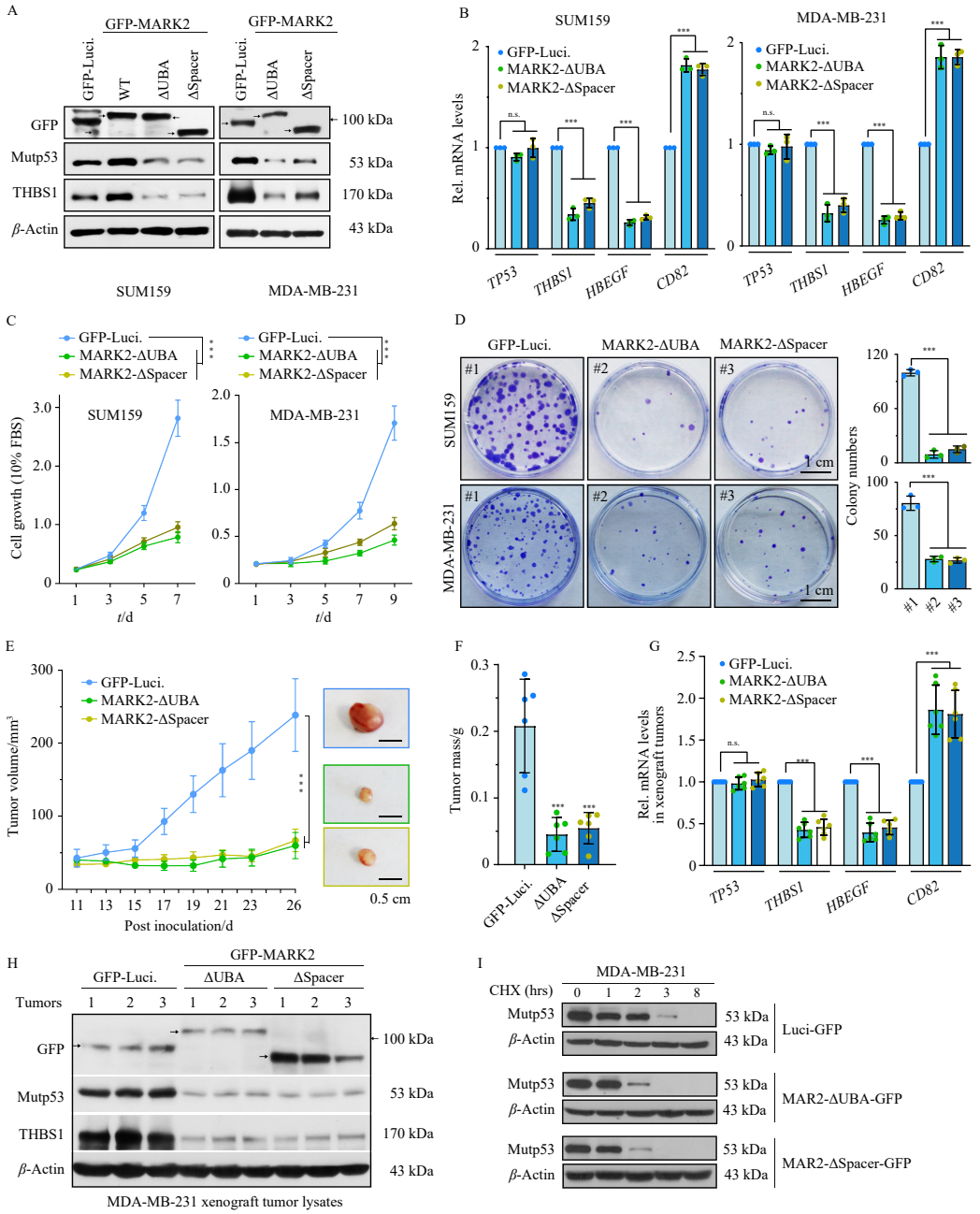

Fig. 6 Ectopic expression of *MARK2*-ΔUBA or *MARK2*-ΔSpacer mutants reduces TNBC progression by inhibiting the mutp53 signaling pathway. (A, B) Immunoblotting (A) and RT-qPCR (B) analyses of MDA-MB-231 and SUM159 cells stably expressing GFP-tagged *MARK2*-WT, *MARK2*-ΔUBA, *MARK2*-ΔSpacer, or luciferase control lentiviral vectors. Asterisks indicate nonspecific bands. (C, D) CCK-8 (C) and colony formation (D) assays evaluating the growth of SUM159 and MDA-MB-231 cells described in (A). (E, F) Tumor growth curves of xenografts generated by subcutaneous inoculation of nude mice with the indicated MDA-MB-231 cells, measured daily (E), and tumor weights at the experimental endpoint (F). (G, H) RT-qPCR (G) and immunoblotting (H) analyses of the indicated genes and proteins in xenograft tumor lysates described in (F). (I) Cycloheximide (CHX, 100 μg·mL^{-1}) chase analysis of mutp53 protein levels in cells overexpressing *MARK2*-ΔUBA or *MARK2*-ΔSpacer versus Luci-GFP. Quantification of mutp53 levels is shown in the lower panels. Data are presented as mean ± SD. n = 3 biological replicates for *in vitro* experiments; n = 6 mice per group for *in vivo* studies. Statistical analysis was performed using one-way ANOVA followed by Dunnett's test (B, D, F, G), longitudinal models for time-course tumor growth (C, E). $^{***}P < 0.001$; n.s., not significant.

ors of *MARK2*.

4. Discussion

In this study, we systematically investigated the roles of MARK family members in triple-negative breast cancer, with a particular focus on their functional interplay with mutant p53. Consistent with this notion, silencing *MARK2* expression markedly suppressed TNBC progression and attenuated mutp53-associated signaling, whereas perturbation of other MARK family members produced distinct or minimal effects. This specificity is supported by previous knockout mouse studies: while *MARK1/3/4*-deficient mice are generally viable, MARK-knockout mice exhibit embryonic lethality and obvious dwarfism and subfertility in female mice, reflecting a broader role in cell fate regulation [41–44]. MARKs, a cytoplasmic serine/threonine protein kinase family, function as conserved regulators of cellular polarity and microtubule dynamics through the phosphorylation of microtubule-associated proteins [20–23]. In addition, MARKs are known to regulate the output of other cytoplasmic signaling pathways linked to cell proliferation and differentiation, including Wnt, AMPK, Hippo, and MAPK [45–48]. Using confocal immunofluorescence combined with nucleocytoplasmic separation experimentation, we unexpectedly observe that *MARK2* is predominantly expressed in the nucleus (with much higher levels than in the cytoplasm), where it colocalizes and physically interacts with

mutp53; however, *MARK1* and *MARK3* are exclusively expressed in the cytoplasm of TNBC cells, without binding with mutp53. The differential cellular localization of *MARK2* versus other MARK family members may explain the observations that only *MARK2* could bind with and stabilize mutp53 protein in the nucleus of TNBC cells, and elevated expression of *MARK2* as well as enhanced *MARK2*/mutp53 signaling promote TNBC progression and are associated with poor clinical outcomes in TNBC patients harboring mut*TP53*. Of note, elevated expression of *MARK2* is not associated with poor prognosis in all three subtypes of breast cancer patients bearing wt*TP53*, which may be attributed to the lack of ability to regulate wtp53 expression by *MARK2*.

Given that the majority of TNBC patients harbor *TP53* mutations, efforts aimed at targeting MARK2/mutp53 signaling pathway may exert unexpected therapeutic benefit in this neoplastic state. Here we have discovered two potent protein-based inhibitors of *MARK2*, *MARK2*-ΔUBA and *MARK2*-ΔSpacer mutant proteins that could effectively reduce TNBC progression through blocking *MARK2*-driven mutp53 signaling. Notably, both mutants lack the ability to bind mutp53 and rescue its stability, as confirmed by domain-specific CHX chase assays. This evidence directly links the physical *MARK2*-mutp53 interaction *via* the UBA and Spacer domains to mutp53 protein stabilization. Given that these domains are poorly conserved among the MARK family (Supplementary Figs. S6D–S6E), this structural uniqueness likely explains the specificity of *MARK2* in mutp53 regulation. Thus, a non-viral, lipid nanoparticle (LNP)-based mRNA delivery of *MARK2*-ΔUBA or *MARK2*-ΔSpacer is worthy of further development and utilization for the treatment of TNBC with an activated *MARK2*/mutp53 signaling.

We demonstrated that ectopic expression of WT *MARK2* or KD mutant stabilized mutp53 protein and thereby enhanced the proliferation of TNBC cells in a comparable fashion, suggesting that *MARK2* promotes TNBC progression independently of its kinase activity. Selective small-molecule inhibitors of MARK family members are currently not available due to the high sequence homology in the catalytic domain across the four family members (Supplementary Fig. S6E). Recently, a small-molecule catalytic inhibitor of *MARK3/4* (the compound has a relatively lower inhibitory activity against *MARK1/2*) has been reported to reduce glioma growth in a subcutaneous model by inducing G_2/M cell cycle arrest and cell apoptosis [49], which is inconsistent with our observation that genetic inhibition of *MARK3* and (or) *MARK4* expression has no impact on TNBC cell growth or migration, suggesting that their roles are likely context-dependent and not essential in mutp53-driven TNBC. *MARK1*, interestingly, exhibited a tumor-suppressive effect in our assays, as its knockdown increased TNBC cell proliferation. This is consistent with some prior reports suggesting *MARK1* may play a role in maintaining epithelial polarity and suppressing oncogenic transformation [50, 51]. Given the high specificity and selectivity of RNAi-mediated knockdown of targeted genes, we presume that the compound exerts its inhibitory effect on tumor growth probably through targeting other uncharacterized molecules rather than *MARK3/4* kinase activity. Actually, in a preliminary study, we discovered that a previously reported pan-MARK inhibitor [52] fails to affect TNBC cell growth. Further, we designed a PROTAC wherein an E3 ligand cereblon (CRBN) was linked to the compound ligand through an oxygen bond and found that treatment of TNBC cells with this PROTAC indeed triggered ubiquitin-dependent degradation of *MARK1*, *MARK2*, and *MARK3*, but still had no obvious impact on the growth of TNBC cells. We believe that this may be due to the concurrent inhibition of *MARK1/2/3* expression, because *MARK2* inhibition reduces TNBC cell proliferation while *MARK1* inhibition enhances cell proliferation. Therefore, it is necessary to develop a specific and effective PROTAC for mut*TP53*-bearing TNBC, in which a newly designed ligand that binds a unique pocket within the UBA or Spacer domain of *MARK2*, regions showing less than 50% sequence homology with the other three MARK family members, is linked to CRBN through an oxygen bond.

5. Conclusion

In summary, this study identifies *MARK2* as a critical and specific regulator of tumor progression in triple-negative breast cancer harboring *TP53* mutations. Elevated *MARK2* expression correlates with poor clinical outcomes in *TP53*-mutant TNBC patients, whereas genetic silencing of *MARK2* suppresses tumor growth both *in vitro* and *in vivo*. Mechanistically, *MARK2* promotes TNBC progression by directly interacting with and stabilizing mutant p53 protein, thereby sustaining mutp53-dependent oncogenic signaling. Notably, this pro-tumorigenic function of *MARK2* is independent of its kinase activity and instead relies on its UBA and Spacer domains, which are structurally divergent from other MARK family members. Collectively, these findings establish *MARK2* as a non-redundant driver of mutp53 signaling in TNBC and highlight the *MARK2*–mutp53 axis as a promising therapeutic vulnerability for *TP53*-mutant breast cancer.

Funding

This work was supported by the National Key Research and Development Program of China (No. 2023YFA1801900), the National Natural Science Foundation of China (Nos. 82125036, 82273964, and 82304538), the Jiangsu Provincial Natural Science Fund for Distinguished Young Scholar (No. BK20230042), and the Jiangsu Funding Program for Excellent Postdoctoral Talent (No. 2023ZB171).

Supporting information

Supplementary data associated with this article can be requested by sending E-mail to the corresponding authors.

Declaration of competing interest

These authors declare no conflict of interest.

Acknowledgement

We thank Prof. ZY Jiang (School of Pharmacy, China Pharmaceutical University) for designing and synthesizing the indicated compounds and PROTACs.

References

1 Bray F, Laversanne M, Sung H, et al. Global cancer statistics 2022: GLOBOCAN estimates of incidence and mortality worldwide for 36 cancers in 185 countries. *CA Cancer J Clin*. 2024;74(3):229-263. https://doi.org/10.3322/caac.21834.
2 Denkert C, Liedtke C, Tutt A, et al. Molecular alterations in triple-negative breast cancer-the road to new treatment strategies. *Lancet*. 2017;389 (10087):2430-2442. https://doi.org/10.1016/S0140-6736(16)32454-0.
3 Sharma P. Biology and management of patients with triple-negative breast cancer. *Oncologist*. 2016;21(9):1050-1062. https://doi.org/10.1634/theoncologist.2016-0067.
4 Wang C, Kar S, Lai XN, et al. Triple negative breast cancer in Asia: an insider's view. *Cancer Treat Rev*. 2018;62:29-38. https://doi.org/10.1016/j.ctrv.2017.10.014.
5 Collignon J, Lousberg L, Schroeder H, et al. Triple-negative breast cancer: treatment challenges and solutions. *Breast Cancer (Dove Med Press)*. 2016;8: 93-107. https://doi.org/10.2147/BCTT.S69488.
6 Wang XK, Zheng SQ, Yang AL, et al. Breast cancer subtypes and the risk of distant metastasis at initial diagnosis: a population-based study. *Cancer Manag Res*. 2018;10, 5329–5338 . https://doi.org/10.2147/CMAR.S176763.
7 Lehmann BD, Pietenpol JA. Identification and use of biomarkers in treatment strategies for triple-negative breast cancer subtypes. *J Pathol*. 2014; 232(2): 142-150 . https://doi.org/10.1002/path.4280.
8 Wang HL, Guo M, Wei HD, et al . Targeting p53 pathways: mechanisms, structures, and advances in therapy. *Signal Transduct Target Ther*. 2023;8(1): 92. https://doi.org/10.1038/s41392-023-01347-1.
9 Kandoth C, McLellan MD, Vandin F, et al. Mutational landscape and

significance across 12 major cancer types. *Nature*. 2013;502(7471):333-339. https://doi.org/10.1038/nature12634.
10 Soussi T, Wiman KG. TP53: an oncogene in disguise. *Cell Death Differ*. 2015;2: 1239-1249. https://doi.org/10.1038/cdd.2015.53.
11 Cancer Genome Atlas Network. Comprehensive molecular portraits of human breast tumours. *Nature*. 2012;490(7418):61-70. https://doi.org/10.1038/nature11412.
12 Olivier M, Hollstein M, Hainaut P. TP53 mutations in human cancers: origins, consequences, and clinical use. *Cold Spring Harb Perspect Biol*. 2010;2: a001008. https://doi.org/10.1101/cshperspect.a001008.
13 Funnell T, O'Flanagan CH, Williams MJ, et al. Single-cell genomic variation induced by mutational processes in cancer. *Nature*. 2022;612(7938):106-115. https://doi.org/10.1038/s41586-022-05249-0.
14 Bareche Y, Venet D, Aftimos P, et al. Unravelling triple-negative breast cancer molecular heterogeneity using an integrative multiomic analysis. *Ann Oncol*. 2018;29(4):895-902. https://doi.org/10.1093/annonc/mdy024.
15 Zhang C, Liu J, Xu DD, et al. Gain-of-function mutant p53 in cancer progression and therapy. *J Mol Cell Biol*.2020;12(9):674-687. https://doi.org/10.1093/jmcb/mjaa040.
16 Bykov VJN, Eriksson SE, Bianchi J, et al. Targeting mutant p53 for efficient cancer therapy. *Nat Rev Cancer*. 2018;18(2):89-102. https://doi.org/10.1038/nrc.2017.109.
17 Chen XH, Zhang TT, Su W, et al. Mutant p53 in cancer: from molecular mechanism to therapeutic modulation. *Cell Death Dis*. 2022;13(11):974. https://doi.org/10.1038/s41419-022-05408-1.
18 Hassin O, Oren M. Drugging p53 in cancer: one protein, many targets. *Nat Rev Drug Discov*. 2023;22(2):27-144. https://doi.org/10.1038/s41573-022-00571-8.
19 Dibra D, Moyer SM, El-Naggar AK, et al. Triple-negative breast tumors are dependent on mutant p53 for growth and survival. *Proc Natl Acad Sci USA*. 2023;120(34):e2308807120. https://doi.org/10.1073/pnas.2308807120.
20 Drewes G, Ebneth A, Preuss U, et al. MARK, a novel family of protein kinases that phosphorylate microtubule-associated proteins and trigger microtubule disruption. *Cell*. 1997;89(2):297-308. https://doi.org/10.1016/s0092-8674(00)80208-1.
21 Hurov JB, Watkins JL, Piwnica-Worms H. Atypical PKC phosphorylates PAR-1 kinases to regulate localization and activity. *Curr Biol*. 2004;14(8):736-741. https://doi.org/10.1016/j.cub.2004.04.007.
22 Biernat J, Wu YZ, Timm T, et al. Protein kinase MARK/PAR-1 is required for neurite outgrowth and establishment of neuronal polarity. *Mol Biol Cell*. 2002;13(11):4013-4028. https://doi.org/10.1091/mbc.02-03-0046.
23 Kemphues K. PARsing embryonic polarity. *Cell*. 2000;101(4):345-348. https://doi.org/10.1016/s0092-8674(00)80844-2.
24 Tassan JP, Le Goff X. An overview of the KIN1/PAR-1/MARK kinase family. *Biol Cell*. 2004;96(3):193-199. https://doi.org/10.1016/j.biolcel.2003.10.009.
25 Drewes G. MARKing tau for tangles and toxicity. *Trends Biochem Sci*. 2004;29 (10):548-555. https://doi.org/10.1016/j.tibs.2004.08.001.
26 Panneerselvam S, Marx A, Mandelkow EM, et al. Structure of the catalytic and ubiquitin-associated domains of the protein kinase MARK/Par-1. *Structure*. 2006;14(2):73-183. https://doi.org/10.1016/j.str.2005.09.022.
27 Sultanakhmetov G, Kato I, Asada A, et al. Microtubule-affinity regulating kinase family members distinctively affect tau phosphorylation and promote its toxicity in a *Drosophila* model. *Genes Cells*. 2024;29:337-346. https://doi.org/10.1111/gtc.13101.
28 Anwar S, Shahwan M, Hasan GM, et al. Microtubule-affinity regulating kinase 4: a potential drug target for cancer therapy. *Cell Signal*. 2022;99:110434. https://doi.org/10.1016/j.cellsig.2022.110434.
29 Kato T, Satoh S, Okabe H, et al. Isolation of a novel human gene, *MARKL1*, homologous to *MARK3* and its involvement in hepatocellular carcinogenesis. *Neoplasia*. 2001;3(1):4-9. https://doi.org/10.1038/sj.neo.7900132.
30 Klingbeil O, Skopelitis D, Tonelli C, et al. MARK2/MARK3 kinases are catalytic codependencies of YAP/TAZ in human cancer. *Cancer Discov*. 2024;14:2471-2488. https://doi.org/10.1158/2159-8290.CD-23-1529.
31 Rubin SM, Sage J, Skotheim JM. Integrating old and new paradigms of G_1/S control. *Mol Cell*. 2020;8(2):183-192. https://doi.org/10.1016/j.molcel.2020.08.020.
32 Ekholm SV, Reed SI. Regulation of G_1 cyclin-dependent kinases in the mammalian cell cycle. *Curr Opin Cell Biol*. 2000;12(1):676-684. https://doi.org/10.1016/s0955-0674(00)00151-4.
33 Suski JM, Braun M, Strmiska V, et al. Targeting cell-cycle machinery in cancer. *Cancer Cell*. 2021;39(6):759-778. https://doi.org/10.1016/j.ccell.2021.03.010.
34 Muller PA, Vousden KH. Mutant p53 in cancer: new functions and therapeutic opportunities. *Cancer Cell*. 2014;25(3):304-317. https://doi.org/10.1016/j.ccr.2014.01.021.
35 Zhou G, Wang JP, Zhao M, et al. Gain-of-function mutant p53 promotes cell growth and cancer cell metabolism *via* inhibition of AMPK activation. *Mol Cell*. 2014;54(6):960-974. https://doi.org/10.1016/j.molcel.2014.04.024.
36 Adorno M, Cordenonsi M, Montagner M, et al. A Mutant-p53/Smad complex opposes p63 to empower TGFbeta-induced metastasis. *Cell*. 2009;137(1):87-98. https://doi.org/10.1016/j.cell.2009.01.039.
37 Escoll M, Gargini R, Cuadrado A, et al. Mutant p53 oncogenic functions in cancer stem cells are regulated by WIP through YAP/TAZ. *Oncogene*. 2017;36:3515-3527. https://doi.org/10.1038/onc.2016.518.
38 Wu J, Liang S, Bergholz J, et al. ΔNp63*α* activates CD82 metastasis suppressor to inhibit cancer cell invasion. *Cell Death Dis*. 2014;5:e1280. https://doi.org/10.1038/cddis.2014.239.
39 Piccolo S, Enzo E, Montagner M. p63, Sharp1, and HIFs: master regulators of metastasis in triple-negative breast cancer. *Cancer Res*. 2013;73(16):4978-4981. https://doi.org/10.1158/0008-5472.CAN-13-0962.
40 Ahn JH, Kim TJ, Lee JH, et al. Mutant p53 stimulates cell invasion through an interaction with Rad21 in human ovarian cancer cells. *Sci Rep*. 2017;7:9076. https://doi.org/10.1038/s41598-017-08880-4
41 Bessone S, Vidal F, Le Bouc Y, et al. EMK protein kinase-null mice: dwarfism and hypofertility associated with alterations in the somatotrope and prolactin pathways. *Dev Biol*. 1999;214:87-101. https://doi.org/10.1006/dbio.1999.9379.
42 Lennerz JK, Hurov JB, White LS, et al. Loss of Par-1a/MARK3/C-TAK1 kinase leads to reduced adiposity, resistance to hepatic steatosis, and defective gluconeogenesis. *Mol Cell Biol*. 2010;30(21):5043-5056. https://doi.org/10.1128/MCB.01472-09.
43 Sun C, Tian L, Nie J, et al. Inactivation of MARK4, an AMP-activated protein kinase (APK)-related kinase, leads to insulin hypersensitivity and resistance to diet-induced obesity. *J Biol Chem*. 2012;287(45):38305-38315 https://doi.org/10.1074/jbc.M112.388934.
44 Fumoto K, Takigawa-Imamura H, Sumiyama K, et al. Modulation of apical constriction by Wnt signaling is required for lung epithelial shape transition. *Development*. 2017;144(1):151-162. https://doi.org/10.1242/dev.141325.
45 Lei YN, Zhang RY, Cai F. Role of MARK2 in the nervous system and cancer. *Cancer Gene Ther*. 2024;31:497-506. https://doi.org/10.1038/s41417-024-00737-z.
46 Lizcano JM, Göransson O, Toth R, et al. LKB1 is a master kinase that activates 13 kinases of the AMPK subfamily, including MARK/PAR-1. *EMBO J*. 2004;23: 833-843. https://doi.org/10.1038/sj.emboj.7600110.
47 Huang HL, Wang SM, Yin MX, et al. Par-1 regulates tissue growth by influencing hippo phosphorylation status and hippo-salvador association. *Plos Biol*. 2013;11(8):e1001620. https://doi.org/10.1371/journal.pbio.1001620.
48 Spilker AC, Rabilotta A, Zbinden C, et al. MAP kinase signaling antagonizes PAR-1 function during polarization of the early *Caenorhabditis elegans* embryo. *Genetics*. 2009;183(3):965-977. https://doi.org/10.1534/genetics.109.106716.
49 Li FF, Liu ZL, Sun HY, et al. PCC0208017, a novel small-molecule inhibitor of MARK3/MARK4, suppresses glioma progression *in vitro* and *in vivo*. *Acta Pharm Sin B*. 2020;10(2):289-300. https://doi.org/10.1016/j.apsb.2019.09.004.
50 Lu X, Chen ZY, Mi WT, et al. MARK1 suppress malignant progression of hepatocellular carcinoma and improves sorafenib resistance through negatively regulating POTEE. *Open Med (Wars)*. 2024;19(1):20241060. https://doi.org/10.1515/med-2024-1060.
51 Tang XL, Yang MY, Wang Z, et al. MicroRNA-23a promotes colorectal cancer cell migration and proliferation by targeting at MARK1. *Acta Biochim Biophys Sin (Shanghai)*. 2019;51(7):661-668. https://doi.org/10.1093/abbs/gmz047.
52 Sloman DL, Noucti N, Altman MD, et al. Optimization of microtubule affinity regulating kinase (MARK) inhibitors with improved physical properties. *Bioorg Med Chem Lett*. 2016;26(17):4362-4366. https://doi.org/10.1016/j.bmcl.2016.02.003.